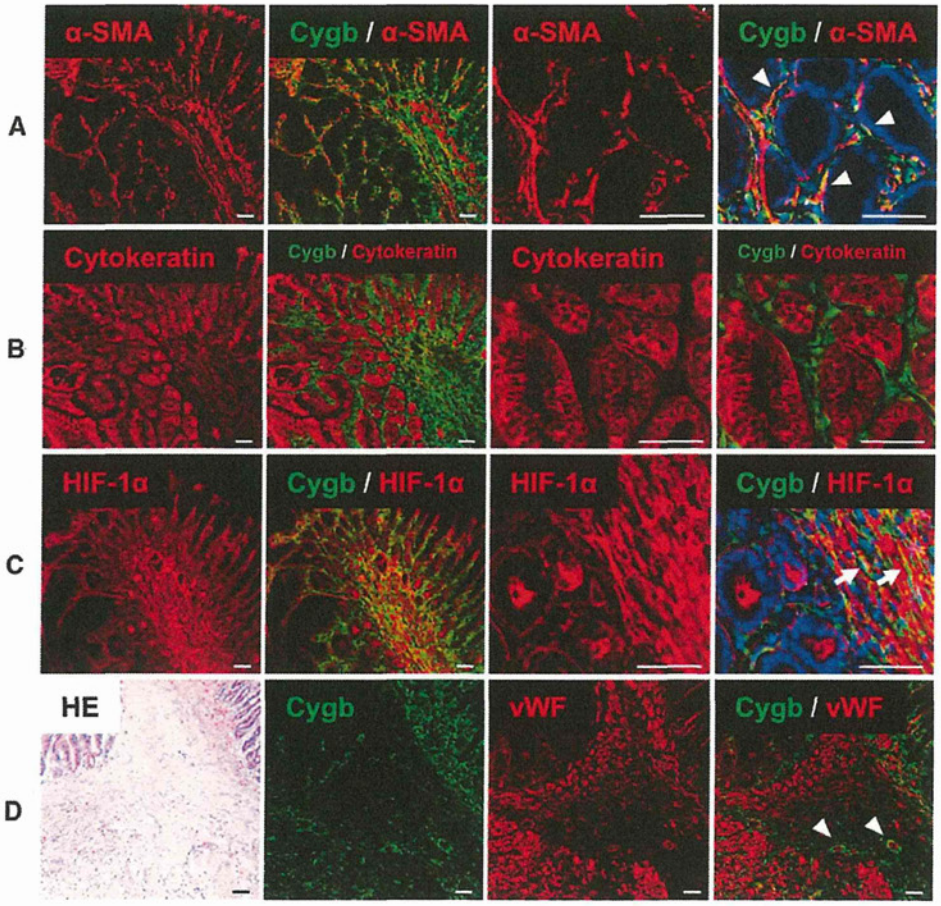

Fig. 4 Immunostaining for Cygb with α-SMA, cytokeratin, HIF-1α and vWF at the marginal zone of the ulcerated tissues. **a** Cygb and α-SMA expressions. Colocalization was observed in the mucosal layer (*first and second panel* from *left*). Highly magnified images showed double-positive cells were linear-shaped cells surrounding the glands which were indicated to be myofibroblasts (*third and fourth panel, arrowheads*). **b** Cygb and cytokeratin expressions. Cygb was not expressed in the epithelial cells which were immunoreactive for cytokeratin. Two panels from *left* are middle magnified and other panels are highly magnified images. **c** Cygb and HIF-1α expressions. HIF-1α was expressed in the mucosal and submucosal layer (*first panel* from *left*). Colocalization of Cygb and HIF-1α was stronger in the submucosal layer than that in the mucosal layer (*second panel*). On highly magnified images, colocalization was observed in the submucosal spindle-shaped cells which were indicated to be fibroblasts (*third and fourth panel, arrows*). **d** Cygb and vWF expressions. Cygb-immunoreactive cells were sparsely observed in the vicinity of vWF-immunoreactive vascular endothelial cells (*arrowheads*). *HE* hematoxylin and eosin. *Scale bars* 50 μm

observed in the vicinity of vascular endothelial cells (vWF-positive cells; Fig. 4d). Cygb was not expressed in the vascular endothelial cells. These results suggested that Cygb was upregulated at the regenerative tissues where angiogenesis had not occurred and it was still under hypoxic condition. However, immunoreactive cells for Cygb were sparse in the area where angiogenesis had already been developed.

Discussion

In this study, we showed that the expression of HIF-1α protein was significantly increased in the early healing phase of gastric ulceration (from day 7 to 11 after the production of gastric ulcer). In contrast, Cygb protein was significantly upregulated in the late healing phase of acute gastric mucosal injury and gastric ulceration (from day 11 to 18). There was a difference between HIF-1α and Cygb protein expression in the time phase. These results showed that Cygb was introduced after the HIF-1α protein stabilization. This is consistent with the previous report which showed that Cygb was regulated by HIF-1α [4, 11]. We finally considered that the healing phase could be divided into two phases; phase 1, early phase (HIF-1α elevating phase, from day 7 to 11); phase 2, late phase (Cygb elevating phase, from day 11 to 18).

Concerning the localization of Cygb, we demonstrated that Cygb was expressed on fibroblasts and myofibroblasts. Cygb was not expressed in the epithelial cells. These results were commonly observed in both an acute gastric mucosal injury model and chronic gastric ulcer model. Moreover, double positive spindle shaped cells for Cygb and HIF-1α were abundantly present at the marginal zone of gastric ulcer, whereas Cygb-immunoreactive cells were not observed in the vicinity of vWF-positive cells. Cygb expression was faint in the regenerative tissues with angiogenesis. From day 11 to 18, Cygb and HIF-1α protein levels were gradually decreased from the peak level observed at day 11. However, VEGF mRNA level was increased in a time-dependent manner from day 11 to 18. VEGF expression peaked at day 18. These characteristic changes of HIF-1α and VEGF expressions during gastric ulcer healing are consistent with the previously reported data [15]. These results suggest that the area with angiogenesis which is mediated by VEGF has not already been under hypoxic condition. In contrast, a hypoxic condition in the ulcerated area triggers HIF-1α induction followed by Cygb induction in the mesenchymal cells like fibroblasts. Accordingly, Cygb is likely to function as a transit oxygen supplier, oxygen sensor, and scavenger of reactive oxygen species in the relatively hypoxic lesion in which angiogenesis has not been completed. Cygb functions as an intracellular oxygen transporter because this protein has 40 % amino acid sequence homology with myoglobin [7]. Fago et al. [6] demonstrated that O_2 binding to Cygb was pH-independent and exothermic throughout the temperature range investigated. These results showed that Cygb might be involved in O_2-requiring metabolic processes. Previous reports showed Cygb might function as a scavenger of reactive oxygen species [4, 5]. Xu et al. [27] demonstrated that an increased expression of Cygb in hepatic stellate cells protected the cells from oxidative stress when exposed to nitrolotriacetate and arachidonic acid, two compounds which induced lipid peroxidation. Besides the heme, other components may also contribute to scavenging for reactive oxygen species (ROS), like reactive thiols, which are readily accessible to oxidizing agents. The exact mechanism by which Cygb protects the cell against oxidative stress-induced cell death remains to be elucidated. In addition, Cygb triggers the transformation of fibroblasts to myofibroblasts that express well-developed actin stress fibers and stimulates collagen production at the inflammatory sites [3]. The extracellular matrix (ECM), including collagen, fibronectin, and laminin, plays an important role in cell adhesion, migration, and proliferation during wound healing [28, 29]. Cygb is associated with ECM synthesis in the healing process and the present time course of Cygb expression was consistent with those of ECM expression needed for ulcer healing in our previous report [24]. Cygb may also play a role as an introducer of tissue fibrosis during the late phase of gastric ulcer healing. Unfortunately we could not investigate the precise role of Cygb in this study. Though Cygb and HIF-1α were colocalized in the cytoplasm of the spindle-shaped cells, there is no direct evidence to indicate that HIF-1α binds to HRF motifs of the *CYGB* gene. Further studies are needed to clarify these problems.

In conclusion, Cygb was mainly expressed on myofibroblasts and fibroblasts and it may be involved in the healing process of gastric mucosal injuries in the late phase when angiogenesis has not been developed. This finding may be helpful for elucidating the mechanism(s) underlying the healing process. Cygb targeting therapy may provide a new strategy for the treatment of various ulcerative diseases.

Conflict of interest None.

References

1. Kawada N, Kristensen DB, Asahina K, et al. Characterization of a stellate cell activation-associated protein (STAP) with peroxidase activity found in rat hepatic stellate cells. *J Biol Chem*. 2001;276:25318–25323.
2. Asahina K, Kawada N, Kristensen DB, et al. Characterization of human stellate cell activation-associated protein and its expression in human liver. *Biochim Biophys Acta*. 2002;1577:471–475.
3. Nakatani K, Okuyama H, Shimahara Y, et al. Cytoglobin/STAP, its unique localization in splanchnic fibroblast-like cells and function in organ fibrogenesis. *Lab Invest*. 2004;84:91–101.
4. Fordel E, Thijs L, Moens L, Dewilde S. Neuroglobin and cytoglobin expression in mice. Evidence for a correlation with reactive oxygen species scavenging. *FEBS J*. 2007;274:1312–1317.
5. Mammen PP, Shelton JM, Ye Q, et al. Cytoglobin is a stress-responsive hemoprotein expressed in the developing and adult brain. *J Histochem Cytochem*. 2006;54:1349–1361.
6. Fago A, Hundahl C, Dewilde S, Gilany K, Moens L, Weber RE. Allosteric regulation and temperature dependence of oxygen binding in human neuroglobin and cytoglobin. Molecular mechanisms and physiological significance. *J Biol Chem*. 2004;279:44417–44426.
7. Burmester T, Ebner B, Weich B, Hankeln T. Cytoglobin: a novel globin type ubiquitously expressed in vertebrate tissues. *Mol Biol Evol*. 2002;19:416–421.
8. Hankeln T, Ebner B, Fuchs C, et al. Neuroglobin and cytoglobin in search of their role in the vertebrate globin family. *J Inorg Biochem*. 2005;99:110–119.
9. Schmidt M, Gerlach F, Avivi A, et al. Cytoglobin is a respiratory protein in connective tissue and neurons, which is up-regulated by hypoxia. *J Biol Chem*. 2004;279:8063–8069.
10. Fordel E, Geuens E, Dewilde S, et al. Cytoglobin expression is upregulated in all tissues upon hypoxia: an in vitro and in vivo study by quantitative real-time PCR. *Biochem Biophys Res Commun*. 2004;319:342–348.
11. Guo X, Philipsen S, Tan-Un KC. Study of the hypoxia-dependent regulation of human CYGB gene. *Biochem Biophys Res Commun*. 2007;364:145–150.

12. Ferrara N. Role of vascular endothelial growth factor in regulation of physiological angiogenesis. *Am J Physiol Cell Physiol.* 2001;280:C1358–C1366.
13. Takahashi M, Kawabe T, Ogura K, et al. Expression of vascular endothelial growth factor at the human gastric ulcer margin and in cultured gastric fibroblasts: a new angiogenic factor for gastric ulcer healing. *Biochem Biophys Res Commun.* 1997;234:493–498.
14. Jones MK, Itani RM, Wang H, et al. Activation of VEGF and Ras genes in gastric mucosa during angiogenic response to ethanol injury. *Am J Physiol.* 1999;276:G1345–G1355.
15. Hashimoto H, Akimoto M, Maeda A, Shigemoto M, Yamashito K. Relation of hypoxia-inducible factor-1alpha to vascular endothelial growth factor and vasoactive factors during healing of gastric ulcers. *J Cardiovasc Pharmacol.* 2004;44:S407–S409.
16. Forsythe JA, Jiang BH, Iyer NV, et al. Activation of vascular endothelial growth factor gene transcription by hypoxia-inducible factor 1. *Mol Cell Biol.* 1996;16:4604–4613.
17. Salceda S, Caro J. Hypoxia-inducible factor 1alpha (HIF-1alpha) protein is rapidly degraded by the ubiquitin-proteasome system under normoxic conditions. Its stabilization by hypoxia depends on redox-induced changes. *J Biol Chem.* 1997;272:22642–22647.
18. Ito M, Tanaka S, Kim S, et al. The specific expression of hypoxia inducible factor-1alpha in human gastric mucosa induced by nonsteroidal anti-inflammatory drugs. *Aliment Pharmacol Ther.* 2003;18:90–98.
19. Baatar D, Jones MK, Tsugawa K, et al. Esophageal ulceration triggers expression of hypoxia-inducible factor-1 alpha and activates vascular endothelial growth factor gene: implications for angiogenesis and ulcer healing. *Am J Pathol.* 2002;161:1449–1457.
20. Semenza GL, Jiang BH, Leung SW, et al. Hypoxia response elements in the aldolase A, enolase 1, and lactate dehydrogenase A gene promoters contain essential binding sites for hypoxia-inducible factor 1. *J Biol Chem.* 1996;271:32529–32537.
21. Watanabe T, Higuchi K, Hamaguchi M, et al. Monocyte chemotactic protein-1 regulates leukocyte recruitment during gastric ulcer recurrence induced by tumor necrosis factor-alpha. *Am J Physiol Gastrointest Liver Physiol.* 2004;287:G919–G928.
22. Taira K, Watanabe T, Tanigawa T, et al. Roles of cyclooxygenase-2 and prostaglandin E receptors in gastric mucosal defense in Helicobacter pylori-infected mice. *Inflammopharmacology.* 2007;15:132–138.
23. Okabe S, Roth JL, Pfeiffer CJ. A method for experimental, penetrating gastric and duodenal ulcers in rats. Observations on normal healing. *Am J Dig Dis.* 1971;16:277–284.
24. Tominaga K, Arakawa T, Kim S, Iwao H, Kobayashi K. Increased expression of transforming growth factor-beta1 during gastric ulcer healing in rats. *Dig Dis Sci.* 1997;42:616–625.
25. Hayakawa T, Fujiwara Y, Hamaguchi M, et al. Roles of cyclooxygenase 2 and microsomal prostaglandin E synthase 1 in rat acid reflux oesophagitis. *Gut.* 2006;55:450–456.
26. Uchida M, Kawano O, Misaki N, Saitoh K, Irino O. Healing of acetic acid-induced gastric ulcer and gastric mucosal PGI2 level in rats. *Dig Dis Sci.* 1990;35:80–85.
27. Xu R, Harrison PM, Chen M, et al. Cytoglobin overexpression protects against damage-induced fibrosis. *Mol Ther.* 2006;13:1093–1100.
28. Grinnell F, Billingham RE, Burgess L. Distribution of fibronectin during wound healing in vivo. *J Invest Dermatol.* 1981;76:181–189.
29. Kurkinen M, Vaheri A, Roberts PJ, Stenman S. Sequential appearance of fibronectin and collagen in experimental granulation tissue. *Lab Invest.* 1980;43:47–51.

Laboratory Investigation (2013) 93, 54–71

Morphological and microarray analyses of human hepatocytes from xenogeneic host livers

Chise Tateno[1,2,3], Fuyuki Miya[4], Kenjiro Wake[5,6], Miho Kataoka[3], Yuji Ishida[1,2], Chihiro Yamasaki[1], Ami Yanagi[1], Masakazu Kakuni[1], Eddie Wisse[7], Fons Verheyen[7], Kouji Inoue[8], Kota Sato[9], Atsushi Kudo[9], Shigeki Arii[9], Toshiyuki Itamoto[10], Toshimasa Asahara[2,10], Tatsuhiko Tsunoda[4] and Katsutoshi Yoshizato[1,2,3,11]

We previously produced mice with human hepatocyte (h-hep) chimeric livers by transplanting h-heps into albumin enhancer/promoter-driven urokinase-type plasminogen activator-transgenic severe combined immunodeficient (SCID) mice with liver disease. The chimeric livers were constructed with h-heps, mouse hepatocytes, and mouse hepatic sinusoidal cells (m-HSCs). Here, we investigated the morphological features of the chimeric livers and the h-hep gene expression profiles in the xenogeneic animal body. To do so, we performed immunohistochemistry, morphometric analyses, and electron microscopic observations on chimeric mouse livers, and used microarray analyses to compare gene expression patterns in hepatocytes derived from chimeric mouse hepatocytes (c-heps) and h-heps. Morphometric analysis revealed that the ratio of hepatocytes to m-HSCs in the chimeric mouse livers were twofold higher than those in the SCID mouse livers, corresponding to twin-cell plates in the chimeric mouse liver. The h-heps in the chimeric mouse did not show hypoxia even in the twin-cell plate structure, probably because of low oxygen consumption by the h-heps relative to the mouse hepatocytes (m-heps). Immunohistochemical and electron microscopic examinations revealed that the sinusoids in the chimeric mouse livers were normally constructed with h-heps and m-HSCs. However, a number of microvilli projected into the intercellular clefts on the lateral aspects of the hepatocytes, features typical of a growth phase. Microarray profiles indicated that ~82% of 16 605 probes were within a twofold range difference between h-heps and c-heps. Cluster and principal component analyses showed that the gene expression patterns of c-heps were extremely similar to those of h-heps. In conclusion, the chimeric mouse livers were normally reconstructed with h-heps and m-HSCs, and expressed most human genes at levels similar to those in human livers, although the chimeric livers showed morphological characteristics typical of growth.

Laboratory Investigation (2013) **93,** 54–71; doi:10.1038/labinvest.2012.158; published online 12 November 2012

KEYWORDS: human hepatocytes; microarray; ultrastructure; uPA/SCID mouse

The liver is a critical organ that can develop a number of serious diseases, including viral hepatitis, alcoholic liver disease, nonalcoholic liver disease, liver cirrhosis, and hepatocarcinoma. From a medical perspective, the liver is also consequential as it can metabolize drugs in the body. Because of differences in liver metabolic function between humans and experimental animals, the results in preclinical efficacy or safety studies using animals do not always apply to humans. On the other hand, although *in vitro* metabolism tests using human hepatocytes (h-heps) have been used to predict the metabolites of new drugs in humans, the results of these studies show limitations in predictivity.[1] For investigating the mechanism of human liver disease and facilitating the development of medicines with high efficacy and safety for

[1]PhoenixBio Co., Ltd., Higashihiroshima, Japan; [2]Hiroshima University Liver Research Project Center, Hiroshima, Japan; [3]Yoshizato Project, Hiroshima Prefectural Institute of Industrial Science and Technology, Cooperative Link of Unique Science and Technology for Economy Revitalization (CLUSTER), Higashihiroshima, Japan; [4]Laboratory for Medical Informatics, Center for Genomic Medicine, RIKEN, Yokohama, Japan; [5]Liver Research Unit, Minophagen Pharmaceutical, Tokyo, Japan; [6]Department of Anatomy, School of Dental Medicine, Tsurumi University, Yokohama, Japan; [7]ELMI unit, Department of Molecular Biology, University Maastricht, Maastricht, The Netherlands; [8]Institute of Electron Microscopy, School of Dental Medicine, Tsurumi University, Yokohama, Japan; [9]Department of Hepatobiliary-Pancreatic Surgery, Graduate School of Medicine, Tokyo Medical and Dental University, Tokyo, Japan; [10]Division of Frontier Medical Science, Department of Surgery, and Hiroshima University 21st Century COE Program for Advanced Radiation Casualty Medicine, Programs for Biomedical Research, Graduate School of Biomedical Sciences, Hiroshima University, Hiroshima, Japan and [11]Developmental Biology Laboratory and Hiroshima University 21st Century COE Program for Advanced Radiation Casualty Medicine, Department of Biological Science, Graduate School of Science, Hiroshima University, Higashihiroshima, Japan
Correspondence: Dr C Tateno, PhD, PhoenixBio Co., Ltd., 3-4-1 Kagamiyama, Higashihiroshima, Hiroshima 7390046, Japan.
E-mail: chise.mukaidani@phoenixbio.co.jp

Received 16 April 2012; revised 24 August 2012; accepted 27 September 2012

humans, humanized animal models are needed, because they represent an approach that can circumvent the limitations of these other methods.

In a previous study, we transplanted h-heps into albumin enhancer/promoter-driven urokinase-transgenic severe combined immunodeficient (uPA/SCID) mice to create h-hep-bearing (chimeric) mice. The host mouse hepatocytes (m-heps) in the livers of the chimeric mice were replaced with h-heps[2] to the degree indicated by the replacement index (RI), which is the occupancy ratio of the h-hep area to the total (human and mouse) area on histological sections. In some cases, the RI in the mice was as high as 96%.[2] The transplanted h-heps expressed mRNA for a variety of human drug-metabolizing enzymes and transporters, in a manner similar to that of the donor liver.[2–4] The chimeric mouse livers were constructed with h-heps, m-heps, and mouse hepatic sinusoidal cells [m-HSCs; mainly Kupffer cells, sinusoidal endothelial cells (SECs), and stellate cells]. Moreover, the hepatocytes cooperated with the m-HSCs in liver function,[5,6] with the h-heps proliferating and functioning under the influence of the xenogeneic m-HSCs. However, few studies have investigated the structure of chimeric mouse livers[7,8] or comprehensively analyzed their gene expression patterns.

The present study was undertaken to study the morphological, biochemical, and genetic similarities or differences between the livers of humans, chimeric mice, and control mice in order to verify whether chimeric mice can be considered to be a relevant model for biomedical experiments concerning the human liver.

MATERIALS AND METHODS

Animals and Transplantation of H-heps

This study was performed with the ethical approval of PhoenixBio, and the Hiroshima Prefectural Institute of Industrial Science and Technology Ethics Board. The uPA/SCID mice were produced as previously described.[2] All transplantation experiments used homozygotic uPA/SCID mice as hosts. Cryopreserved h-heps from a 9-month-old Caucasian boy (9MM) were purchased from In Vitro Technologies (Baltimore, MD, USA). Cryopreserved h-heps from a 5-year-old African-American boy (5YM), a 2-year-old Caucasian boy (2YM), a 4-year-old Caucasian girl (4YF), a 6-year-old African-American girl (6YF), and a 10-year old Caucasian girl (10YM) were purchased from BD Biosciences (San Jose, CA, USA). These h-heps were used as donor cells for chimeric mice.

For the transplantation study, 1 or 2 tubes of cryopreserved h-heps ($5–15 \times 10^6$ cells/vial) were thawed and transplanted into 10–50 uPA/SCID mice ($2.5–10.0 \times 10^5$ viable cells/mouse). The human albumin (hAlb) concentration in the blood samples was periodically measured using latex agglutination immunonephelometry (LX Reagent 'Eiken' Alb II; Eiken Chemical, Tokyo, Japan) to predict the RI of h-heps in mouse livers.[2] The hAlb concentration in mouse blood correlated well with the RI. Chimeric mice (Table 1) were selected from each transplantation study for immunohistochemistry and enzyme histochemistry, blood flow measurements, oxygen consumption studies, electron microscopic examination, blood biochemistry, microarray analysis, and real-time quantitative reverse transcription-PCR (real-time qRT-PCR) analysis.

Immunohistochemistry and Enzyme Histochemistry

Frozen sections were prepared from the livers of 5YM-, 9MM-, and 2YM-chimeric mice (Table 1a, nos. 1–6), SCID mice, and humans (Table 1b). The sections were fixed in –20 °C acetone for 5 min, and then incubated with anti-human cytokeratin (CK) 8/18 (h-hep marker protein), anti-mouse CK18 (m-hep marker protein), BM8 (a mouse macrophage-specific antigen), anti-mouse stabilin II (mouse liver endothelial marker protein),[9] anti-desmin (stellate cell marker protein), anti-type IV collagen, anti-ZO-1, anti-claudin-1, and anti-occludin antibodies (tight junction proteins) (Table 2). The primary antibodies were visualized with Alexa 488- or 594-conjugated donkey anti-mouse-IgG, goat anti-rat IgG, or donkey anti-rabbit IgG (Invitrogen, Carlsbad, CA, USA) as secondary antibodies. The samples were then stained with Hoechst 33258 for nuclear staining. Human CK8/18 antibodies reacted with h-heps, but not m-heps; mouse CK18, BM8, and stabilin II antibodies reacted with m-cells, but not h-cells. Other antibodies reacted with both m- and h-cells (Table 2). Dipeptidyl dipeptidase IV (DPPIV) enzyme histochemistry was performed on liver cryosections as previously shown.[10]

Morphometric Analysis of Liver Cells

Three 5YM-chimeric mice (Table 1a, nos. 1–3) and 3 SCID mice were used in this study. To identify hepatocytes, liver cryosections from chimeric and SCID mice were stained with human CK8/18 and mouse CK18 antibodies, respectively, as above. Frozen sections from both mice were stained with BM8, anti-mouse stabilin II, and desmin antibodies. The numbers of h-heps and m-heps in an arbitrary area were counted as human CK8/18- or mouse CK8-positive cells, respectively. The number of Kupffer cells, SECs, and stellate cells in an arbitrary area were counted as BM8-, mouse-stabilin II-, and desmin-positive cells, respectively. The number of h-heps or m-heps, mouse Kupffer cells, mouse SECs, and mouse stellate cells in a unit area were calculated, and the ratios of component cells in the chimeric and SCID mouse livers were expressed as circle graphs.

Hypoxyprobe-1 treatment

To determine whether h-heps in the chimeric mouse livers were hypoxic, uPA/SCID mice transplanted with h-heps (5YM) or m-heps were injected with 60 mg/kg body weight pimonidazole HCl from the Hypoxyprobe-1 kit (Hypoxyprobe, Burlington, MA, USA), at 3 and 2 weeks after transplantation, respectively. The livers were subsequently

Table 1 Human liver tissues and chimeric mice used in this study

(a) Chimeric mice

Donors	*n*	Animal number (sex)	Weeks after transplantation	hAlb in blood (mg/ml)	RI (%)[a]	Purpose
5YM	3	1 (M), 2 (M), 3 (F)	13–15	12.2–16.5	87–95	Morphometric analysis, immunohistochemistry
9MM	2	4 (M), 5 (F)	11	3.1, 7.4	53, 75	Immunohistochemistry, enzyme histochemistry
2YM	1	6 (F)	10	13.3	97	Immunohistochemistry
5YM	3	7–9 (M)	14	8.2–11.4	75–85	ICG treatment
5YM	3	10–12 (M)	10	8.5–9.6	76–80	Microcirculation
5YM	3	13 (M), 14 (M), 15 (F)	11–14	15.9–17.5	94–97	Oxygen consumption
4YF	2	16 (F), 17 (M)	10, 16	7.5, 7.2	75, 74	Transmission electron microscopy
10YM	2	18 (M), 19 (F)	8	4.1, 4.9	57, 63	Transmission electron microscopy
2YM	2	20 (M), 21 (F)	12, 15	5.6, 11.6	69, 90	Scanning electron microscopy
9MM	3	22–24 (F)	10–14	6.0–16.1	70–95	Microarray, real-time qRT-PCR
6YF	3	25 (F), 26 (F), 27 (M)	11–12	11.2–14.6	91–100	Microarray
5YM	5	28–32 (M)	13 ± 1	11.1 ± 2.4	81 ± 6	Blood chemistry
5YM	5	33–37 (F)	13 ± 2	8.0 ± 1.3	71 ± 5	Blood chemistry

(b) Human liver tissues

Donors	Age (years)	Sex	Purpose
25YF	25	F	Microarray, real-time qRT-PCR, Immunohistochemistry
28YM	28	M	Microarray, real-time qRT-PCR
57YM	57	M	Microarray, real-time qRT-PCR
61YF	61	F	Microarray, real-time qRT-PCR

Abbreviations: F, female; hAlb, human blood albumin; M, male; RI, replacement index.
[a]RI calculated with blood hAlb levels using the formula of the correlation curve for each donor cell.

Table 2 Antibodies for immunohistochemistry

Antibodies	Clone	Host	Specificity	Dilution	Supplier
hCK8/18	Monoclonal	Mouse	h	100	Cappel Laboratory, (Cochranville, PA, USA)
mCK18	Monoclonal	Mouse	m	1	Progen Biotechnik. (Heidelberg, Germany)
BM8	Monoclonal	Rat	m	1000	BMA Biomedicals, (Augst, Switzerland)
mStabilin II	Monoclonal	Rat	m	1000	Gift from Dr Miyajima, (Tokyo University, Japan)
Desmin	Polyclonal	Rabbit	h, m	500	SYNBIO (Heidelberg, Germany)
Type IV collagen	Polyclonal	Rabbit	h, m	500	LSL (Tokyo, Japan)
ZO-1	Polyclonal	Rabbit	h, m	50	Zymed Laboratories (South San Francisco, CA, USA)
Claudin-1	Polyclonal	Rabbit	h, m	50	Zymed Laboratories
Occludin	Polyclonal	Rabbit	h, m	100	Zymed Laboratories

Abbreviations: h, human specific; m, mouse specific.

harvested at 1 h after the injection. Chimeric mice (5YM, nos. 1–3) at 13–15 weeks after transplantation and 14-week-old SCID mice were also treated with pimonidazole HCl in the same manner. Acetone-fixed, frozen liver sections were treated with anti-pimonidazole adduct mouse monoclonal antibodies and biotin-conjugated anti-mouse IgG (Hypoxyprobe-1 kit) and diaminobenzidine according to the manufacture's protocol.

Blood flow measurements

Indo-cyanine green (ICG, MP Biomedicals, LLC) dissolved in distilled water was injected into 3 chimeric mice (5YM, nos. 7–9) and 3 SCID mice via the tail vein at 25 mg/kg body weight. Blood was collected at 0, 2, 3, 4, 5, 6, 9, 12, 24, and 60 min after the injection, and the ICG concentrations were measured in the sera by the microplate reader system Vmax (Molecular Device, Ontario, Canada). The blood flow was calculated by moment analysis.

The microcirculation of the livers in 3 chimeric (5YM, nos. 10–12) and 3 SCID mice was observed under anesthesia using intravital videomicroscopy, as described previously.[11] For analyzing sinusoidal blood flow, at least 3 different sinusoids per mouse were captured in the microscopic fields at 500 frames/s using high-speed progressive videomicroscopy (HAS-LI, DITECT, Tokyo, Japan). This system enables high-resolution (1920 × 1080) capture of real-time red blood cell flow in the sinusoid, with the hydrodynamics analyzed by the Flowsizer 2D software (DITECT).

Measurement of Oxygen Consumption in H-Heps and M-Heps

Chimeric mouse hepatocytes (c-heps) and m-heps were isolated by the collagenase perfusion method from three 5YM-chimeric mice (nos. 13–15) and three SCID mice, respectively, as below. Donor hepatocytes (5YM), c-heps, and m-heps (1.5×10^6 cells) were incubated in 5 ml of 10 mM glucose in Dulbecco's modified Eagle's medium with 10% fetal bovine serum at 37 °C. Oxygen concentrations were measured every 5 min until 20 min using a SG6-ELK Professional dissolved oxygen meter (Mettler-Toledo KK, Tokyo, Japan). The oxygen consumption rate was calculated based on the oxygen concentration at each time point.

Electron Microscopy

The 4YF- and 10YM-chimeric mouse livers (Table 1a, nos. 16–19) were harvested under anesthesia. The mouse livers were prefixed by perfusing 1.5% glutaraldehyde in 0.1 M cacodylate buffer (pH 7.4) through a portal vein at 4 °C for 40 s using a syringe. The livers were cut into 1-mm^3 blocks with a razor blade under the affluent solution in 2% glutaraldehyde/0.1 M cacodylate buffer (pH 7.4). Next, the sample blocks were postfixed with 1% OsO_4/0.1 M phosphate buffer (pH 7.4) for 1 h at 4 °C. After the blocks were washed with 0.1 M phosphate buffer (pH 7.4), they were dehydrated through an ethanol series and propylene oxide, and embedded in Epon.[12] Ultrathin sections were cut with a Reichert Ultracut ultramicrotome (Reichert Optikwork, Vienna, Austria), stained with lead and uranyl salts, and examined in a JEOL-100 CX TEM (Tokyo, Japan) operated at 80 kV.

For scanning electron microscopy (SEM), the livers of 2YM-chimeric mice (Table 1a, nos. 20 and 21) were perfused through a portal vein with filtered 1.5% glutaraldehyde under anesthesia, and then with 1% sucrose/0.067 M cacodylate buffer (pH 7.4) at room temperature for 5 min.[13] The livers were cut into 1 × 1 × 5 mm blocks with a razor blade under the fixative solution, and washed with 1% sucrose/0.067 M cacodylate buffer (pH 7.4). The blocks were postfixed with 1% OsO_4/0.1 M phosphate buffer (pH 7.4) for 1 h at 4 °C, and then washed with 0.1 M phosphate buffer (pH 7.4). They were dehydrated with an ethanol series. After being treated with 100% ethanol, the samples were immersed for 10 min in 100% hexamethyldisilazane (Sigma Chemical), and dried in a desiccator. The samples were then mounted on stubs and sputter-coated with 10 nm of gold. They were observed under an SEM (model XL30, Philips).

Isolation of H-Heps from Human and Chimeric Mouse Livers for Microarray and Real-Time qRT-PCR Analyses

Livers were obtained from 4 individuals: 2 men aged 28 and 57 years (28YM and 57YM, respectively) and 2 women aged 25 and 61 years (25YF and 61YF, respectively; Table 1b). The donors gave informed consent before surgery, according to the 1975 Declaration of Helsinki. The h-heps were isolated from these tissues, as previously reported,[2] and subjected to microarray and real-time qRT-PCR analyses (Table 1b). The c-heps were isolated from 9MM-chimeric mice (Table 1a, nos. 22–24) 10–14 weeks after transplantation and 6YF-chimeric mice (Table 1a, nos. 25–27) 11–12 weeks after transplantation. These animals had high (>70%) RI levels (Table 1a). The livers were disaggregated using the two-step collagenase perfusion method:[14] the livers were perfused for 20 min, and then centrifuged 3 times at 50 *g* for 2 min. The hepatocytes obtained as pellets from the c-heps were used for the microarray and real-time qRT-PCR analyses. The cells were frozen in liquid nitrogen and stored in a deep freezer until total RNA isolation.

Microarray Analysis

Microarray-based gene expression analysis was performed at the hepatocyte level using c-heps or h-heps as RNA sources. Four human individuals (25YF, 28YM, 57YM, and 61YF; Table 1b) and 6 chimeric mice (Table 1a, nos. 22–27) were used in the microarray assay.

Total RNA was isolated from each hepatocyte sample using TRIzol reagent (Invitrogen), treated with DNase (Qiagen), and purified using the RNase-Free DNase Set (Qiagen) and the RNeasy Mini Kit (Qiagen). The RNAs from c-heps or h-heps were applied to the microarray assay using GeneChip Human Genome U-133 Plus 2.0 Array (Affymetrix, Santa Clara, CA, USA) with 54 675 probe sets according to the manufacturer's instructions. The obtained mRNA expression profiles (c-heps, $n=6$; h-heps, $n=4$) are designated as the hepatocyte-level profiles in this study. The gene expression array data were normalized using the MAS5 algorithm (Affymetrix). The signal reliability of each probe was determined based on the MAS5 Call algorithm (Affymetrix), and each probe was assigned to 1 of 3 flags (P, present; M, marginal; and A, absent). For correcting bias between chips, quantile normalization[15] was applied to all array data using

R software. We deposited our array data to NCBI GEO (Gene Expression Omnibus, http://www.ncbi.nlm.nih.gov/geo/, GEO ID GSE33846, GSE18674).

For determining the similarity of c-heps and h-heps, the microarray data of c-heps, h-heps, and 22 human tissues (h-tissues) (liver, kidney, pancreas, cerebellum, cortex, fetal brain, spinal cord, bone marrow, heart, skeletal muscle, salivary gland, colon, stomach, small intestine, lung, uterus, prostate, thyroid, trachea, spleen, thymus, and testis) were analyzed using principle component analysis (PCA) for 46 336 probes that were assigned as positive (P flag) for at least one of the flags in any of c-heps, h-heps, or 22 h-tissues, including h-liver. PCA and cluster analysis were performed using GeneSpring GX 11.0 (Agilent Technologies) and R software.

Liver signature probes were selected as follows: 685 and 805 probes with expression levels twofold higher or lower in the h-liver than in all of the other 21 h-tissues were selected among the 54 675 probes as liver high signature probes (Supplementary Table 1) and liver low signature probes (data not shown), respectively. The results of Gene Ontology (GO) and pathway analysis indicated that the selected 685 probes represent liver-specific components (Supplementary Table 2). Cluster analysis was performed with the average linkage method and Euclidian distance using Cluster and TreeView.[16]

Determination of mRNA Expression Levels by Real-Time qRT-PCR Analysis

A total of 17 human genes (*IGF-1*, *SOCS2*, *NNMT*, *IGFLS*, *KLOTHO*, *P4AH1*, *SLC16A1*, *SRD5A1*, *SCD*, *FADS1*, *FADS2*, *FASN*, *DGAT2*, *ADPN*, *SREBP1c*, *FABP*, and *AKR1B10*) were selected based on a previous study.[17] That is, these genes were previously determined to be up- or down-regulated in chimeric mouse livers when chimeric mice were administered human growth hormone (hGH).[17] The mRNA expression levels of these genes were quantified by real-time qRT-PCR. The specimens used for the microarray analysis were used for the extraction of total RNA, which was performed as described above. cDNA was synthesized using 1 μg of RNA, PowerScript reverse transcriptase (Clontech, Mountain View, CA, USA), and oligo-dT primers (Invitrogen) according to the manufacturer's instructions, and then subjected to real-time qRT-PCR. Genes were amplified with a set of gene-specific primers[17] and SYBR Green PCR mix in a PRISM 7700 Sequence Detector (Applied Biosystems, Tokyo, Japan). We confirmed conditions consisted of an initial denaturation step at 95 °C for 10 min, followed by 40 cycles at 95 °C for 15 s, and 60 °C for 1 min. All data were calculated by the comparative threshold cycle (Ct) method as previously described.[18] Contamination by m-heps did not affect the RT-PCR determination of human gene expression because the expression level of each gene was normalized against the human glyceraldehyde 3-phosphate dehydrogenase (hGAPDH) gene.

Gene Enrichment Analysis

Gene and GO information was collected from NCBI build 37 (http://ncbi.nlm.nih.gov) and the GO (http://www.geneontology.org) sites, respectively. Pathway information was collected from KEGG (http://www.genome.jp/kegg) and the Ingenuity Pathways Analysis (IPA) software (Ingenuity Systems). The gene enrichment analysis was performed using only GO and the pathway group when at least two or more genes were assigned.

Biochemical Tests

Blood was collected from the inferior vena cava of 5 male and 5 female 5YM-chimeric mice (Table 1a, nos. 28–37), 5 male uPA/SCID mice, and 3 male SCID mice at the time of killing. The sera were used for the following biochemical tests: glutamic pyruvic transaminase (GPT), glutamic oxaloacetic transaminase (GOT), γ-glutamyltransferase (GGT), cholinesterase (CHE), blood urea nitrogen (BUN), total cholesterol (TCHO), high-density lipoprotein cholesterol (HDL-c), triglycerides (TGs), total bilirubin (TBIL), glucose (GLU), total albumin (ALB), and total protein (TP). These tests were conducted using a Fuji Drichem 3500 V serum analyzer (Fujifilm, Tokyo, Japan).

Statistical Analyses

Microarray data were evaluated by Welch's *t*-test (two-sided) and adjusted for multiple testing using the Benjamini–Hochberg (B–H) false discovery rate (FDR).[19] The gene enrichment analysis and the significance of overlap between two groups of transcripts were performed using Fisher's exact test, and the gene enrichment analysis was corrected with the B–H FDR.[19] Data obtained in blood chemistry were analyzed among groups by ANOVA. When the overall F-statistics were significant, significance was determined by Sheffe's test with significance level $\alpha = 0.05$.

RESULTS

Construction of Chimeric Mouse Livers with H-Heps and M-HSCs

Cryopreserved donor hepatocytes (5YM) were thawed and transplanted into 54 2–4-week-old uPA/SCID mice (2.5×10^5 cells/animal), and blood hAlb concentrations were monitored (Figure 1a). In all, 50 mice remained alive beyond 10 weeks of age. Of these, 1, 3, and 2 mice showed 1–3, 3–5, and 5–7 mg/ml hAlb blood concentrations, respectively, at 10 weeks of age. Also, 44 mice secreted >7 mg/ml hAlb into the blood, and 6 mice died after reaching 10 weeks of age (5–7 mg/ml, $n=1$; >7 mg/ml hAlb, $n=5$). Three mice showing >7 mg/ml hAlb were used for morphometric analysis (nos. 1–3, Figure 1b and c). Immunohistochemistry showed that the hepatocytes and the nuclei were smaller in the chimeric mice than in the SCID mice (Figure 2a and b), which were similar to the h-heps in a human body (data not shown). BM8-positive mouse Kupffer cells (Figure 2c and d), desmin-positive mouse stellate cells (Figure 2g and h), and

m-Stabilin II-positive m-SECs (Figure 2e and f) were uniformly distributed in both livers, but their densities were lower in the chimeric mice than in the SCID mice. Desmin-positive mouse stellate cells with cytoplasmic projections were closely associated with the m-SECs (data not shown).

The BM8-positive mouse Kupffer cells were smaller in the chimeric mice ($39.2 \pm 4.3\,\mu m^2$) than in the SCID mice ($50.6 \pm 4.0\,\mu m^2$; Figure 2c and d). Moreover, large BM8-positive cells were occasionally present near portal veins in the chimeric mice (data not shown).

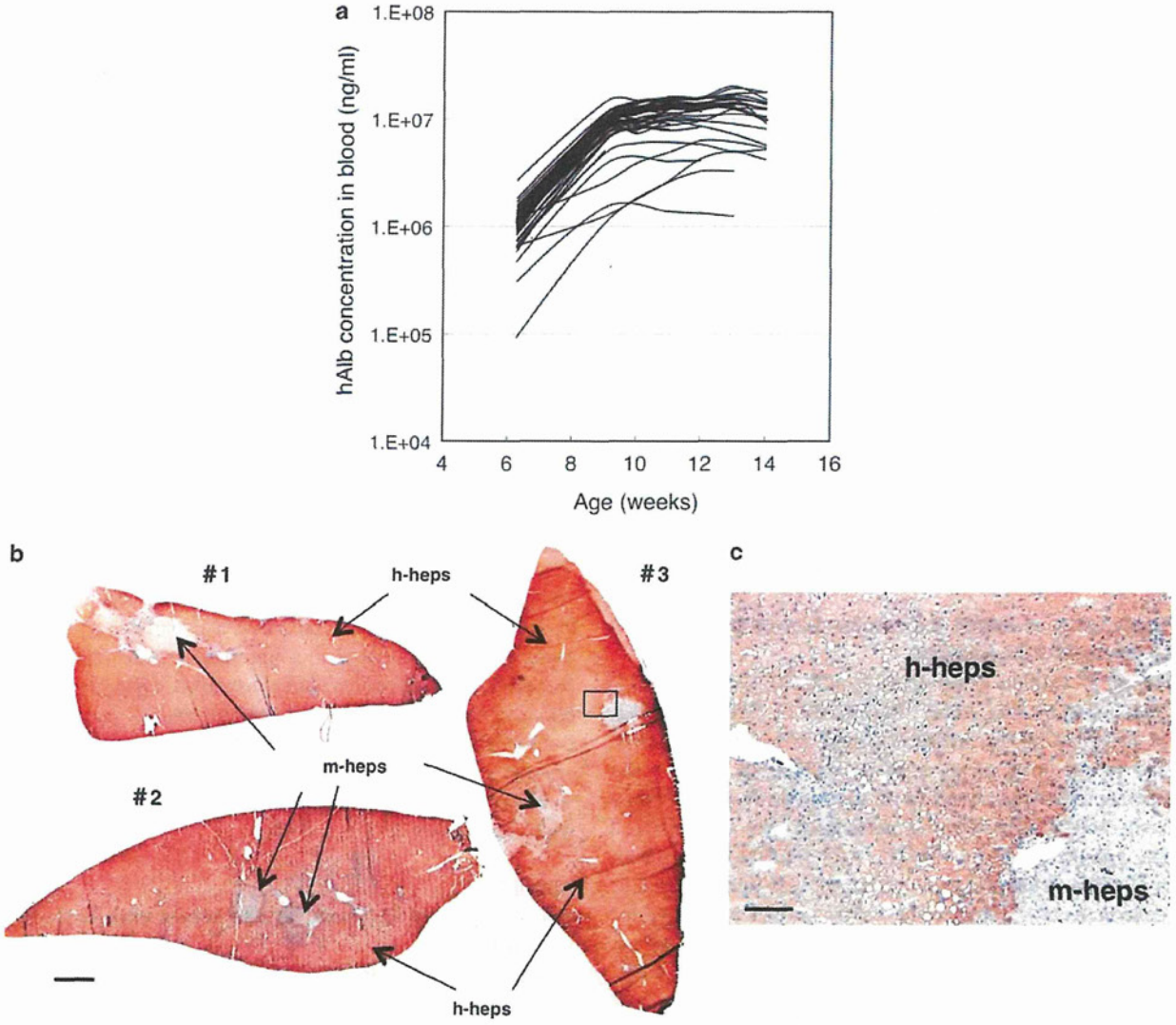

Figure 1 Changes in hAlb concentration in the blood and immunostained livers of mice transplanted with h-heps. (**a**) The graph shows an example of the results of the transplantation of h-heps into uPA/SCID mice. The h-heps from 5YM were transplanted into 54 uPA/SCID mice, and the hAlb concentrations in mouse blood were monitored. A total of 50 mice remained alive beyond 10 weeks of age. Of these, 1, 3, and 2 mice showed 1–3, 3–5, and 5–7 mg/ml hAlb concentrations, respectively, after 10 weeks of age. Forty-four mice leached >7 mg/ml hAlb into the blood, which corresponds to >70% RI. Three 5YM-chimeric mice were used for morphometric analysis. (**b**) The livers of three 5YM-chimeric mice (nos. 1–3) were immunostained with human CK8/18 antibodies. The brown-colored area is that of h-heps. The mouse livers were almost entirely repopulated by h-heps. Bar = 1 mm. (**c**) A magnified view of the liver region enclosed by the square for chimeric mouse no. 3 of (**b**). Bar = 100 μm.

Figure 2 Immunohistochemistry of SCID and chimeric mouse liver for morphometric analysis. Three SCID (**a**, **c**, **e**, **g**) and 5YM-chimeric mouse (**b**, **d**, **f**, **h**) livers were stained with Hoechst 33248 and m-CK18 (**a**) or h-CK8/18 (**b**); BM8 (**c**, **d**); anti-mouse stabilin II (**e**, **f**); desmin and m-CK18 (**g**) or h-CK8/18 (**h**). The cells and nuclei in the SCID mice were larger than those in the chimeric mice (**a**, **b**). The densities of BM8-, anti-mouse stabilin II-, and desmin-positive cells were lower in the chimeric mice than those in the SCID mice (**c**–**h**). BM8-positive cells were smaller in the chimeric mice than those in the SCID mice (**c**, **d**). Magnification is identical for panels belonging to the same horizontal pair. Bar = 100 μm.

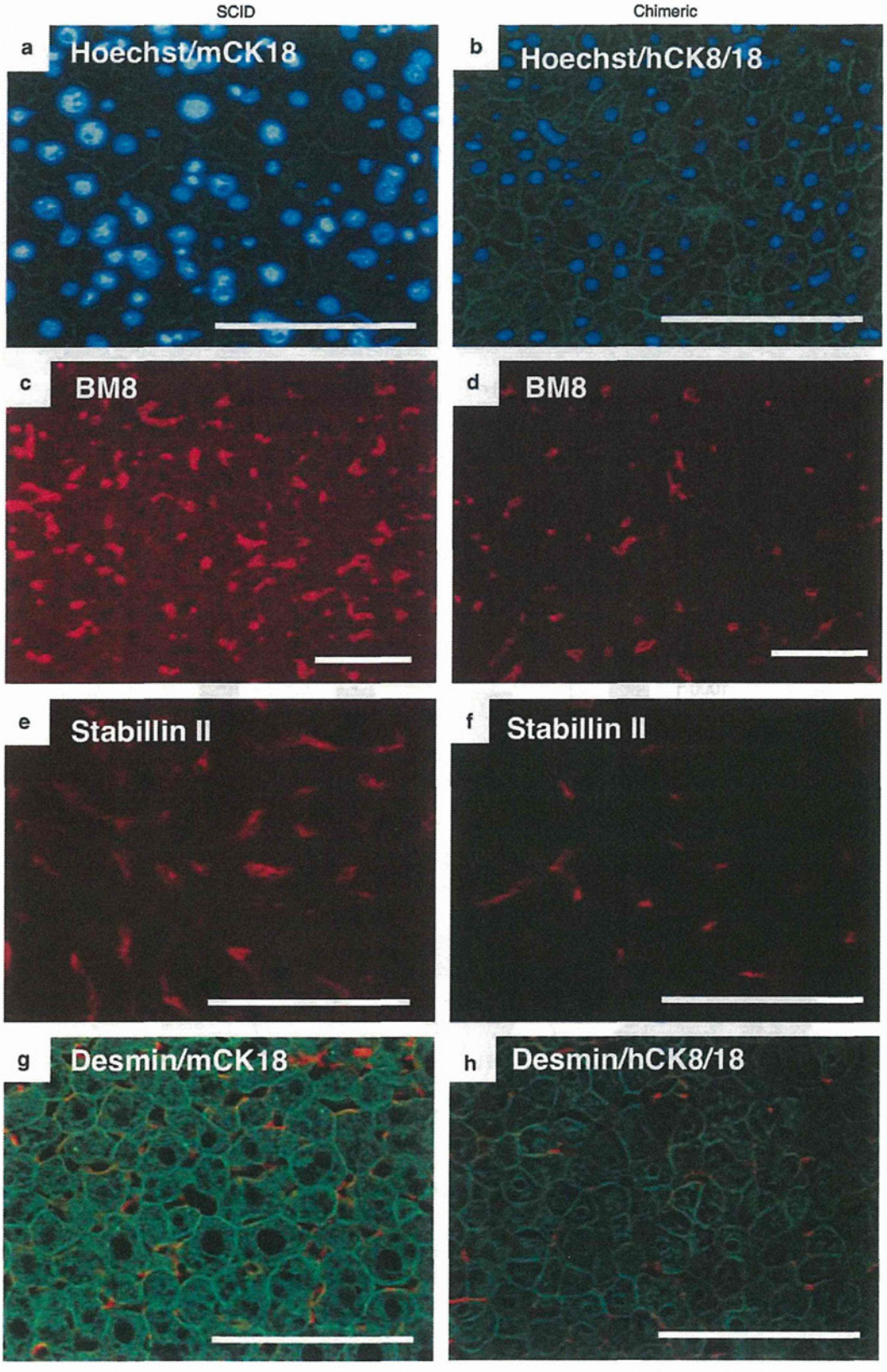

Figure 2 For caption please refer page 59.

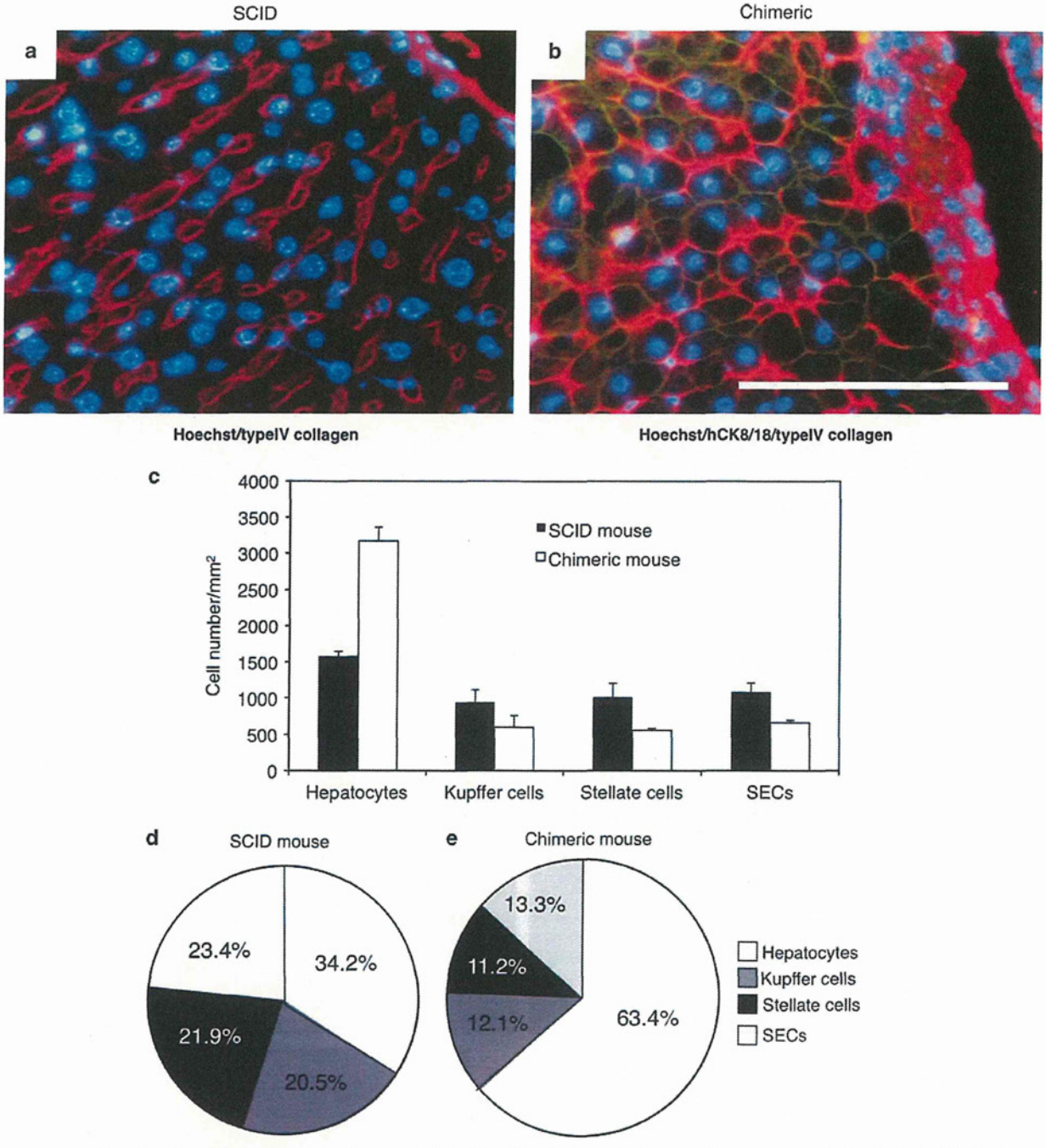

Figure 3 Immunohistochemistry of chimeric mouse livers stained for Type IV collagen, and the ratio of component cells in SCID (**a**) and chimeric (**b**) mouse livers. SCID and 5YM-chimeric mouse livers were stained with Hoechst and anti-type IV collagen antibody. 5YM-chimeric mouse livers were additionally stained with human CK8/18 antibodies. SCID and chimeric mouse livers showed single-cell and twin-cell plates, respectively. Bar = 100 μm. The number of hep cells, BM8-positive cells (Kupffer cells), desmin-positive cells (stellate cells), and anti-mouse stabilin II-positive cells (SECs) were counted under a microscope, and the density of each cell type was calculated (**c**). The ratios of the component cells in SCID (**d**) and chimeric mice (**e**) were calculated from the data of (**c**), and expressed as circle graphs. The ratios of Kupffer cells, stellate cells, and SECs were similar in the SCID and chimeric mice, but the ratio of hepatocytes to HSCs (Kupffer cells, stellate cells, and SEC) was twofold greater in the chimeric mice than that in the SCID mice.

Type IV collagen depositions were observed on the basal aspect of the heps (Figure 3a and b). In the SCID mouse liver, the m-heps showed single-cell plates (Figure 3a), whereas the h-heps in the chimeric mouse liver showed twin-cell plates (Figure 3b). The h-heps or m-heps in combination with the m-HSCs (m-Kupffer cells, m-SECs, and m-stellate cells)

were counted in an arbitrary area on samples from three chimeric mice or three SCID mice, respectively (Figure 3c), and the ratios were subsequently compared (Figure 3d and e). The ratios of the Kupffer cells, SECs, and stellate cells were similar between groups. However, the ratios of the h-heps and m-HSCs in the chimeric mice were twofold greater than those in the SCID mice (Figure 3d and e).

Lack of Hypoxia in H-Heps with Twin-Cell Plates

To determine whether the h-heps with the twin-cell plates were in a hypoxic state, the chimeric mice were treated with hypoxyprobe-1. The result revealed that the m-heps in the 14-week-old SCID mouse liver (Figure 4a) and the h-heps in the chimeric mouse liver at 13–15 weeks after transplantation (growth termination phase, Figure 4b) did not show hypoxia. The growing m-heps at 2 weeks after transplantation in the uPA/SCID mouse liver showed hypoxia (Figure 4c), whereas the growing h-heps at 3 weeks after transplantation did not show hypoxia (Figure 4d). The host uPA/SCID mouse hepatocytes (Figure 4c and d) were damaged and atrophic because of the expression of uPA. Thus, our results suggest that the damaged uPA/SCID mouse liver might be hypoxic.

As determined by measuring ICG concentrations, the liver blood flow was similar between the SCID and chimeric mice (Figure 4e and f), suggesting that the overall blood flow within the liver was similar between these two groups of mice. The livers of the chimeric mice were enlarged, with the liver weight to body weight ratio at $13.0 \pm 0.3\%$ for the chimeric mice and at $5.4 \pm 0.5\%$ for the SCID mice.[20] The microcirculation of the SCID and chimeric mice livers were then determined in order to investigate the effects of the enlarged liver size on sinusoidal blood flow in the chimeric mouse liver. The blood cell flow rate was slower in the sinusoids of the chimeric mouse liver ($0.0116 \pm 0.003\ \mu m/\mu s$, Figure 4g) than in those of the SCID mouse liver ($0.0247 \pm 0.005\ \mu m/\mu s$, Figure 4g). In addition, no disturbances were observed in the microcirculation of either the SCID or chimeric mice livers, despite the blood flow in the chimeric mouse liver occurring at half the rate seen in the SCID mouse liver.

The oxygen consumption of the c-heps increased in a cell number-dependent manner (Figure 4h). Moreover, the oxygen consumption of 1.5×10^6 m-heps was higher than that of 5.0×10^6 c-heps (Figure 4h). The oxygen consumption rates of m-heps from SCID mice, h-heps from chimeric mice, and donor h-heps from the chimeric mice were 4.82 ± 0.25, 1.07 ± 0.13, and $0.54\ \mu M/ml/10^6$ cells, respectively (Figure 4i).

Ultrastructure of Chimeric Mouse Livers

The chimeric mouse livers were found to be composed of three visually identifiable regions of different colors.[1] The white and red regions corresponded to the original diseased m-heps and uPA gene-deleted m-hep regions, respectively. The medium-toned regions between the white and red regions corresponded to h-heps. Electron microscopic observation showed that the h-heps in the medium-colored regions were distinguished as cells with abundant glycogen and large lipid droplets in the cytoplasm (Figure 5a). In contrast, abundant small granules (0.1–0.5 μm in diameter) were observed in the original diseased m-hep cells in the white regions (Figure 5b). M-heps in the red regions showed a normal morphology (Figure 5c).

The space of Disse was observed between the h-heps and the SECs of the mouse liver (Figure 5a), whereas bile canaliculi were seen between the h-heps (Figure 5d). In the space of Disse, stellate cells with lipid droplets were observed (Figure 5e). Meanwhile, SEM revealed fenestrae in the SECs (Figure 5f). The h-heps adhered to each other and formed bile canaliculi on the apical surfaces, whereas their basal surfaces had many microvilli facing the thin mouse SECs (Figure 5a and d). These results indicate normal reconstruction of the chimeric mouse livers with h-heps and m-HSCs.

Cell–Cell Adhesion Between Hepatocytes

In chimeric mouse livers, immunocytochemistry detected tight junction proteins, such as ZO-1 (Figure 6a), claudin-1 (data not shown), and occludin-1 (Figure 6c), on membranes adjacent to h-heps, as would occur in the human liver (Figure 6b and d). However, the frequency was lower in the chimeric mouse livers than in the human ones. DPPIV activity was observed on the microvilli of bile canaliculi (Figure 6f). In the chimeric mouse livers, DPPIV enzyme activity was concentrated on membranes adjacent to the h-heps. Interestingly, faint signals were detected on the h-hep cell surfaces near portal veins in the chimeric livers (Figure 6e).

Bile canaliculi are organized by junctional complexes. Electron microscopic examination demonstrated that junctional complexes, consisting of tight junctions, adherence

Figure 4 Analyses of pimonidazole binding (**a–d**), blood flow (**e–g**), and oxygen consumption (**h, i**) in SCID and chimeric mouse livers. SCID and chimeric mice and uPA/SCID mice transplanted with m-heps (2 weeks after transplantation) and h-heps (3 weeks after transplantation) were injected with pimonidazole HCl; the livers were then immunostained for pimonidazole adducts. SCID (**a**) and chimeric mouse livers (**b**) were negative for the adducts, whereas uPA/SCID mouse hepatocytes were positive for pimonidazole adducts (**c, d**). M-hep-colonies (**c**, arrowheads) were positive, whereas h-hep-colonies were negative (**d**, arrowheads). Bar = 100 μm. The chimeric mice and SCID mice were injected with ICG. The ICG concentrations in the mouse sera were subsequently monitored (**e**). The clearance rate of ICG was similar between the SCID and chimeric mice (**f**). The sinusoidal blood flow in the chimeric mouse liver was approximately one-half of that in the SCID mouse liver (**g**). The oxygen consumption of c-heps and m-heps was monitored (**h**). The oxygen consumption of c-heps was 1/4.5 lower than that of m-heps. $^*P<0.05$, $^{**}P<0.01$.

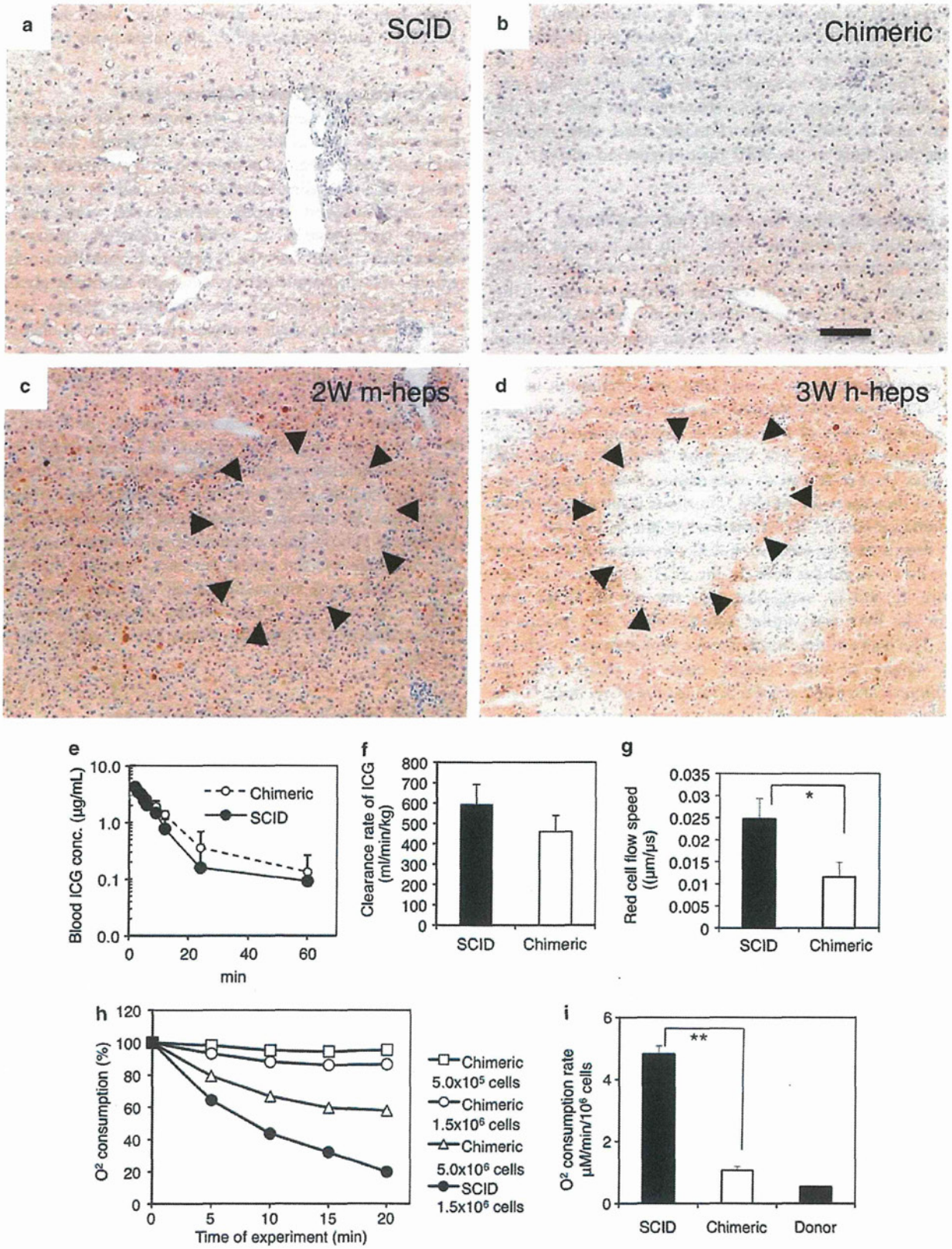
a
SCID
b
Chimeric
c
2W m-heps
d
3W h-heps
e
Blood ICG conc. (μg/mL)
10.0
1.0
0.1
0.0
Chimeric
SCID
0
20
40
60
min
f
Clearance rate of ICG (ml/min/kg)
800
700
600
500
400
300
200
100
0
SCID
Chimeric
g
Red cell flow speed ((μm/μs)
0.035
0.03
0.025
0.02
0.015
0.01
0.005
0
*
SCID
Chimeric
h
O² consumption (%)
120
100
80
60
40
20
0
0
5
10
15
20
Time of experiment (min)
Chimeric 5.0x10⁵ cells
Chimeric 1.5x10⁶ cells
Chimeric 5.0x10⁶ cells
SCID 1.5x10⁶ cells
i
O² consumption rate μM/min/10⁶ cells
6
4
2
0
**
SCID
Chimeric
Donor

junctions, and desmosomes, directly adjoined bile canaliculi between h-heps (Figure 7a). In rare cases, bile canaliculi were also formed between h-heps and m-heps (Figure 7b). In the peripheral areas of the cytoplasm in groupings of two h-heps and one m-hep, many microvilli projected into the intercellular clefts on the lateral aspects of the hepatocytes (Figure 7c). A small number of cone-like cytoplasmic processes formed contacts with neighboring cells, not only between h-heps (Figure 7c) but also between m-heps and h-heps (Figure 7d). Electron microscopic observation showed gap junctions between h-heps (Figure 7e) and between m-heps (data not shown).

Changes in Blood Biochemistry by Repopulation of Mouse Liver with H-Heps

Sera of the chimeric (Table 1a), uPA/SCID, and SCID mice were biochemically tested (Table 3). The data for the normal range in humans[21,22] are also shown in Table 3. GOT and GPT were higher in the chimeric and uPA/SCID mice than in the normal mice because of the liver damage by uPA expression in the m-heps.[2] GGT was significantly higher in the chimeric mice than in the SCID mice and the normal human samples.[21] CHE activity differed between humans and male SCID mice (660–1620 IU/l[22] and 18 IU/l, respectively). CHE activity in the male chimeric mice was ~400 IU/l. These data indicate that the c-heps synthesized and secreted GGT and CHE in the same manner as human hepatocytes. HDL-c and low-density lipoprotein cholesterol (LDL-c) ratios also differed between humans and mice. HDL-c was higher than LDL-c in the SCID mice, whereas LDL-c was higher than HDL-c in humans.[22] LDL-c was higher than HDL-c in the chimeric mice (data not shown), but the HDL-c value was lower than that of normal humans (Table 3). ALB was higher in humans than in mice. Similarly, ALB was higher in the chimeric mice than in the SCID mice, indicating that the sera in the chimeric mice may have been acquiring human characteristics. The biomarkers BUN, TCHO, TG, TBIL, GLU, and TP did not significantly differ between male chimeric and male SCID mice.

Comparison of Gene Expression Profiles in Hepatocytes Isolated from Chimeric Mouse and Human Livers

The mRNA expression profiles of c-heps and h-heps were compared. The c-heps were isolated from three 9MM- and 6YF-chimeric mice (Table 1a), whereas h-heps were isolated from four human liver tissues (Table 1b). The gene profiles were determined for the two types of hepatocytes using microarrays representing 54 675 human transcripts. Among these, 16 605 transcripts (30% of total probes) were assigned as present (P flag) for either all of the c-heps or all of h-heps, and 81.9% were expressed at similar levels (<2-fold difference) in the two types of hepatocytes.

The data for c-heps and h-heps (25YF, 28YM, 57YM, and 61YF) and the 22 h-tissues were clustered for 46 336 probes. The cluster analysis showed that 6 c-heps formed a cluster, and the 4 h-heps and h-liver formed another cluster, with these two clusters closest among the h-tissues (Supplementary Figure 1). PCA was performed for 46 336 probes. PCA showed that the 6 c-heps and 4 h-heps were extremely close to each other, and that the h-liver was the closest to the cluster of the 6 c-heps and 4 h-heps among h-tissues (Figure 8a). We also performed cluster analysis using the 685 liver high signature probes and the 805 liver low signature probes for c-heps, h-heps, and the 22 h-tissues. The cluster analysis demonstrated a close association among c-heps, h-heps, and h-liver (Figure 8b). Pearson's correlation coefficient was calculated for the expression levels of the liver-specific genes (685 probes), resulting in 0.812–0.909 for h-heps *vs* c-heps, 0.881–0.959 for h-heps *vs* h-heps, and 0.903–0.970 for c-heps *vs* c-heps.

The ratios of gene expression levels in the c-heps to those in the h-heps were compared using the data from the microarray and real-time qRT-PCR analyses. The expression levels of 17 genes were divided according to those of h-*GAPDH*. The microarray and real-time qRT-PCR data were well correlated (Spearman's correlation coefficient by rank test = 0.975; Figure 8c).

Moreover, of the 16 605 transcripts, 436 transcripts (2.6%) were twofold lower in expression in the c-heps than in the h-heps ($P<0.05$, two-sided Welch's *t*-test). Of the same total, 197 transcripts (1.2%) showed twofold greater expression in the c-heps than in the h-heps ($P<0.05$; Supplementary Table 3).

DISCUSSION

We morphometrically determined the structure of chimeric mouse livers, clarified the ratios of their component cells (heps, Kupffer cells, SECs, and stellate cells), and determined their morphological relationships through immunohistochemistry and electron microscopy. We recently reported that BrdU incorporation into h-heps was ~6% at 2 or 3 weeks after transplantation, had decreased thereafter, and had dropped to ~2% at 7 and 9 weeks after transplantation. At 11 weeks after transplantation, BrdU

Figure 5 Ultrastructure of the chimeric mouse livers as revealed by TEM (**a–e**) and SEM (**f**). The h-heps contained abundant glycogen and the presence of lipid droplets (**a**, **d**), whereas the mouse hepatocytes damaged by uPA expression showed an abundance of small granules (indicated by the arrow in the inset; **b**). The mouse hepatocytes normalized by deletion of the uPA gene showed a normal structure (**c**). Bile canaliculi formed on the apical membranes of adjacent human hepatocytes, (**d**) and sinusoidal structures were observed on the basal cell membranes (**a**, **d**). A hepatic stellate cell containing lipid droplets was observed in the space of Disse (**e**). Fenestration was normally seen on SECs (**f**). Bar indicates 1 μm in (**a–c**, **e**, **f**); 0.5 μm in the squares of (**b**); and 5 μm in (**d**). BC, bile canaliculi; BL, blood cell; HSC, hepatic stellate cell; L, lipid droplets; M, mitochondria; SD, sinusoid; SEC, sinusoidal endothelial cell.

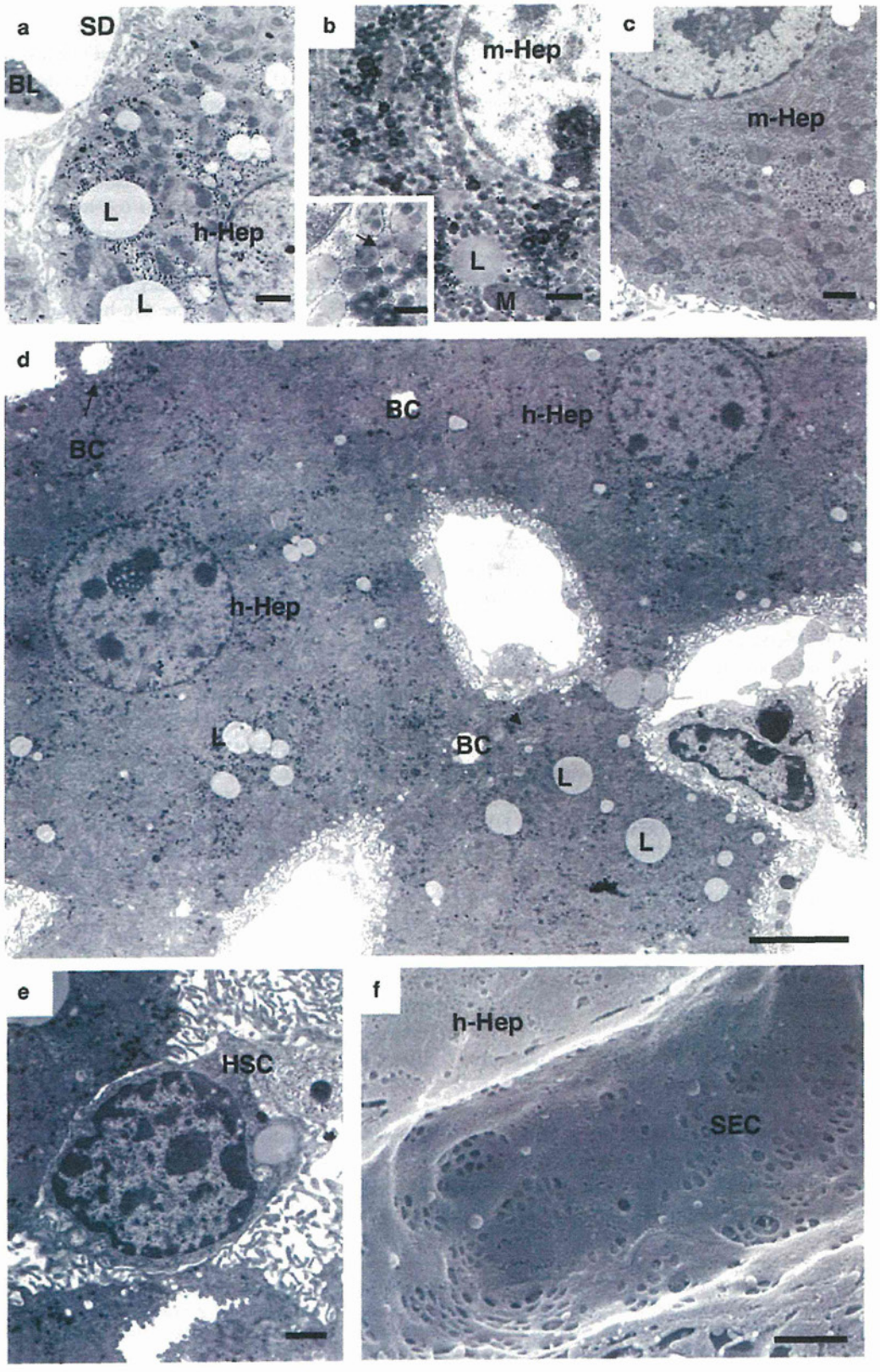
a
SD
BL
L
h-Hep
L
b
m-Hep
L
M
c
m-Hep
d
BC
h-Hep
BC
h-Hep
L
BC
L
L
e
HSC
f
h-Hep
SEC

incorporation was ~1%, which was the same as the control level in adult SCID mouse livers.[20] We also demonstrated that the liver weight to body weight ratios of chimeric mouse livers were ~2 times greater than those of normal mice when the transplants terminated proliferation.[20] These results were considered to indicate hyperplasia of the h-heps, as no significant differences in cell size were observed.[20] The mRNAs of proliferating h-heps contained lower levels of TGF-β type I receptors (TGFBR1), TGFBR2, and activin A type IIA receptors (ACVR2A) than that of resting h-heps from human livers (normal levels), and these levels remained low when the transplants terminated proliferation.[20] Therefore, we suggested that the chimeric mouse livers terminated their growth because of contact inhibition of h-heps or other mechanisms without the TGF-β signaling pathway. From these data, we determined that the h-heps in the chimeric mouse livers were not completely in the G0 stage. The h-heps in the chimeric mouse livers showed twin-cell plates, indicating that some of the proliferating features continued as in regenerating or neonatal livers.[20] In the present study, the morphometric analysis revealed similar HSC ratios in chimeric and SCID mice but an h-hep ratio in the chimeric mouse livers that was twofold higher than that in the SCID mouse liver, corresponding to the twin-cell plates in the chimeric mouse liver. The liver blood flow rate was similar between the SCID and chimeric mice. On the other hand, sinusoidal blood flow in the chimeric mouse was approximately one-half of that in the SCID mouse, probably because of the enlargement of the chimeric mouse liver. However, no disorders in the microcirculation of the chimeric mouse liver were observed. The oxygen consumption rate of hepatocytes is known to be negatively correlated with the average body weights of different species.[23] Using a formula showing the relationship between resting hepatocyte oxygen consumption (y) and body weight (x) ($y=7.09x$),[23] the ratio of the hepatocyte oxygen consumption of mouse (body weight: 0.02 kg) to that of human (body weight: 60 kg) is ~5. In the present study, the oxygen consumption of h-heps was 1/4.5 of m-heps, which was very close to the above calculated rate.

After partial hepatectomy, the division of heps resulted in twin-cell plates, and the heps subsequently showed hypoxia.[24] HIF-1 induction induced expression of downstream genes, such as VEGF and TGF-β3.[24] The author suggested that hypoxia of the heps induced reconstruction from twin-cell plates into single-cell plates by growth of the SECs.[24] hHIF-1α, hVEGF, and hTGF-β3 mRNA expression levels in the chimeric mouse livers were lower than those in human livers by real-time qRT-PCR (data not shown). In the present study, no evidence was found that the h-heps showed hypoxia in the chimeric mouse liver. This finding suggests that the h-heps in the chimeric mice may not be hypoxic, even in the twin-cell plates, because of low oxygen consumption in these cells.

With electron microscopic observation, we were able to easily distinguish h-heps from m-heps in the white areas because of the highly expressed uPA gene. The h-heps showed abundant glycogen and large lipid droplets, whereas m-heps in the white areas had abundant small vesicles in the cytoplasm. Distinguishing h-heps from m-heps in the red areas was difficult because of the deletion of the uPA gene. M-heps retained quantities of glycogen particles, and careful observation of m-heps in the red areas revealed prominent peroxisomes and fewer lipid droplets in the uPA-gene-deleted m-heps than in the h-heps. On the other hand, very few peroxisomes were present in the h-heps. Junctional complexes and bile canaliculi were frequently observed between h-heps in the chimeric mouse livers. In rare cases, bile canaliculi were formed between h-heps and m-heps. In the peripheral cytoplasmic areas of two adjacent h-heps or a h-hep and a m-hep, abundant microvilli projected into the intercellular clefts on the lateral aspects of the hepatocytes. These characteristic morphological features have been frequently observed in regenerating livers.[25] The formation of junctional complexes and bile canaliculi between m-heps and h-heps is an important finding that demonstrates the ability of the mouse bile duct system to extract bile produced by the h-heps. Electron microscopic examination further revealed that SECs and stellate cells existed normally along hepatic cell plates. Fenestration was observed on the SECs in the chimeric mouse livers. These results indicate that chimeric mouse livers showed twin-cell plates like those often seen in regenerating and neonatal livers, whereas h-heps and m-HSCs were normally reconstructed in the chimeric mouse livers.

The present study is the first to compare the gene expression patterns of c-heps and h-heps using microarray analysis. Approximately 82% were expressed at similar levels (<2-fold difference) in the two types of hepatocytes. There was the possibility that mouse transcripts were also included as cDNAs hybridized in the currently adopted microarray assay. Our previous study indicated that the RI represented a lower estimation of the real h-hepatocyte purity in hepatocyte preparations because m-heps were often lost during collagenase digestion because of fragility against the enzyme. The correct h-hepatocyte purity in the c-heps was $90.8 \pm 6.4\%$ ($n=10$).[17] We further checked the cross-hybridization of the cDNAs of the mouse livers and found that 5643 of 54 675 (10.3%) transcripts were positive. As a whole, the presence of m-heps in the c-heps at <10% did not affect the microarray assays in the present study.[17] PCA and cluster analyses showed that the gene expression patterns of the c-heps were extremely similar to those of the h-heps. These data support our previous finding that c-heps retain phenotypes similar to those of h-heps, including *P*450 (CYP), phase II enzymes, and transporters.[2–4] The c-hep samples and h-hep samples are clearly distinct with the 'normal' liver. One possible explanation is that the normal liver tissue contains both h-heps and h-HSCs. Using Fisher's test, we also analyzed 46 336 probes that were assigned as

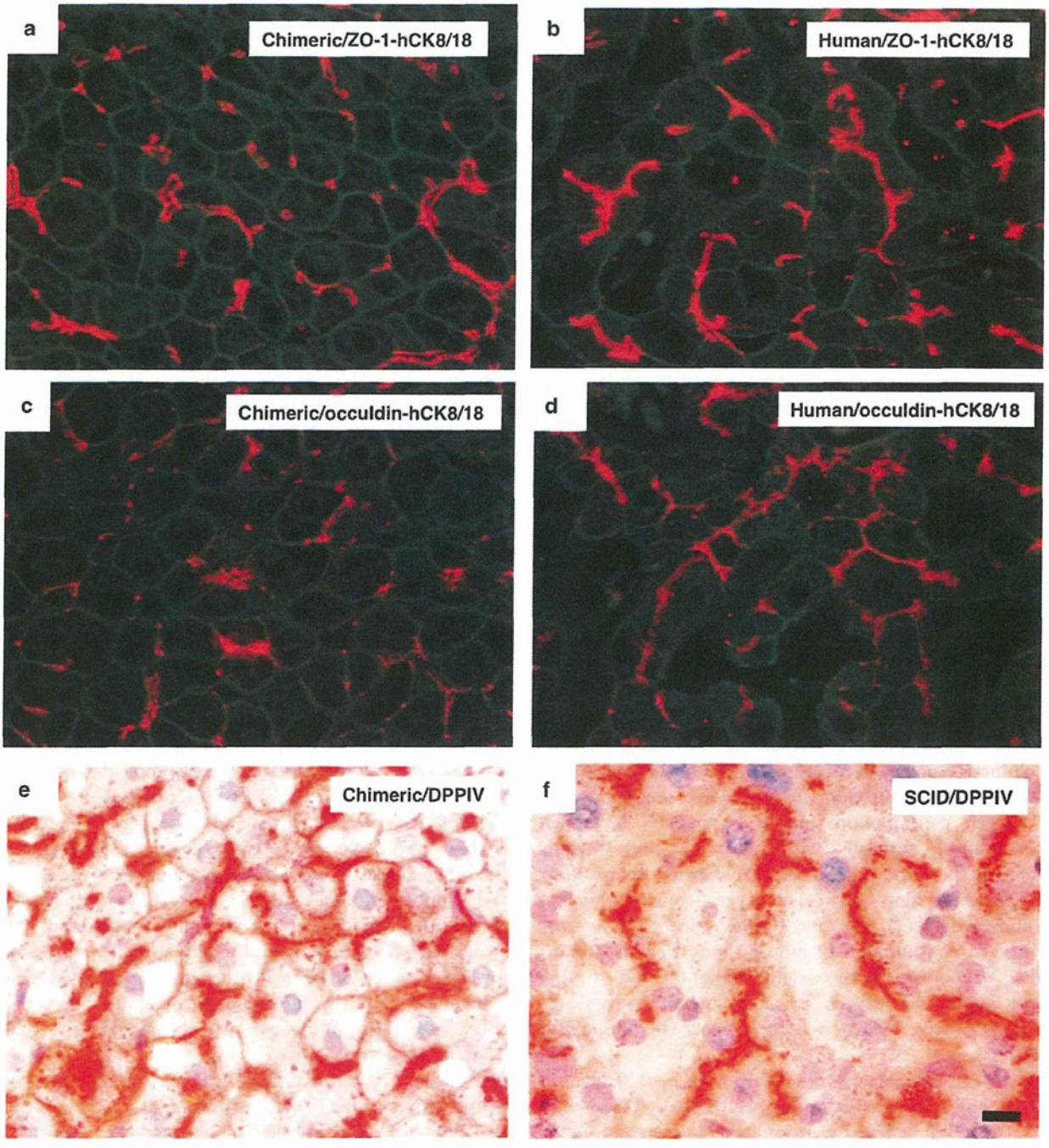

Figure 6 Immunohistochemistry of proteins related to cell adherence in human and chimeric mouse livers, and enzyme histochemistry of DPPIV in SCID and chimeric mouse livers. 9MM-chimeric mouse and human liver sections were stained with ZO-1 (**a**, **b**) and occludin (**c**, **d**) antibodies and stained for DPPIV (**e**, **f**). These proteins were located between hepatocytes in the chimeric mouse livers (**a**, **c**) and the human livers (**b**, **d**). Fewer occludin deposits were observed in the chimeric mouse livers (**c**) than in the human livers (**d**). DPPIV-positive signals were located on the basal membranes in the SCID mice (**f**), but were also observed at the peripheries of human hepatocytes in chimeric mice (**e**). Bar = 10 μm. Magnification is the same in all panels.

positive (P flag) for at least one of the flags in any of the c-heps, h-heps, or 22 h-tissues (Supplementary Table 4). The overlap *P*-values and odds ratio were determined between the liver signature probes and the probes of the h-heps with signals more than 2 times higher or lower compared with the average signals of all the tissues. The number of overlap probes were found to be 539–642 among 685 probes in the liver high expression signature, and the overlap *P*-values in the liver high

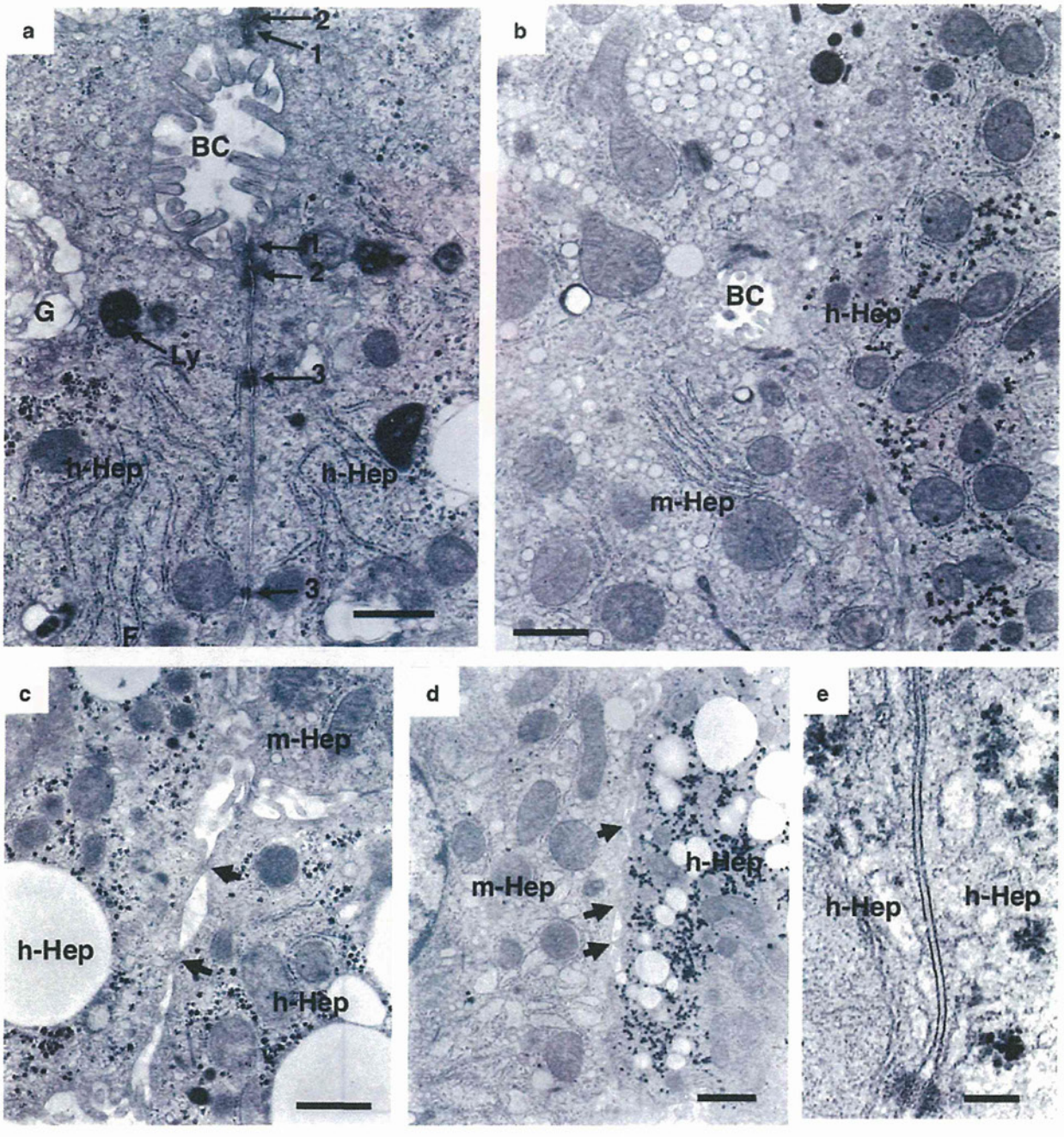

Figure 7 Ultrastructure of cell–cell contact in the chimeric mouse livers. Bile canaliculi were observed between adjacent h-heps (**a**) and between h- and m-heps (**b**) in the 4YF-chimeric mouse liver, as well as junctional complexes (tight junction, 1; adherence junction, 2; desmosome, 3). In the peripheral cytoplasmic areas of groups formed by two adjacent human hepatocytes and one m-hep, many microvilli projected into the intercellular clefts on the lateral aspects of the hepatocytes (**c**). We judged that the left and right cells in (**b**) are m-hep damaged by uPA expression and h-hep, respectively, because many membrane-limited granules are scattered throughout the cytoplasm in the left cell and the presence of abundant glycogen particles is observed in the cytoplasm in the right cell. A small number of cone-like cytoplasmic processes made contact with neighboring cells (**c, d**). Gap junctions were frequently observed between human hepatocytes (**e**). Bar = 0.5 μm in (**a**); 1 μm in (**b, c, d**); and 0.1 μm in (**e**). BC, bile canaliculi; G, Golgi complex; Ly, lysosome.

expression signature were $<2.2 \times 10^{-16}$. The number of overlap probes were 153–485 among 805 probes in the liver low expression signature and were fewer than in the liver high expression signature; however, the overlap *P*-values in the liver low expression signature were also $<2.2 \times 10^{-16}$. From these data, we observe that the c-hep samples, h-hep samples,

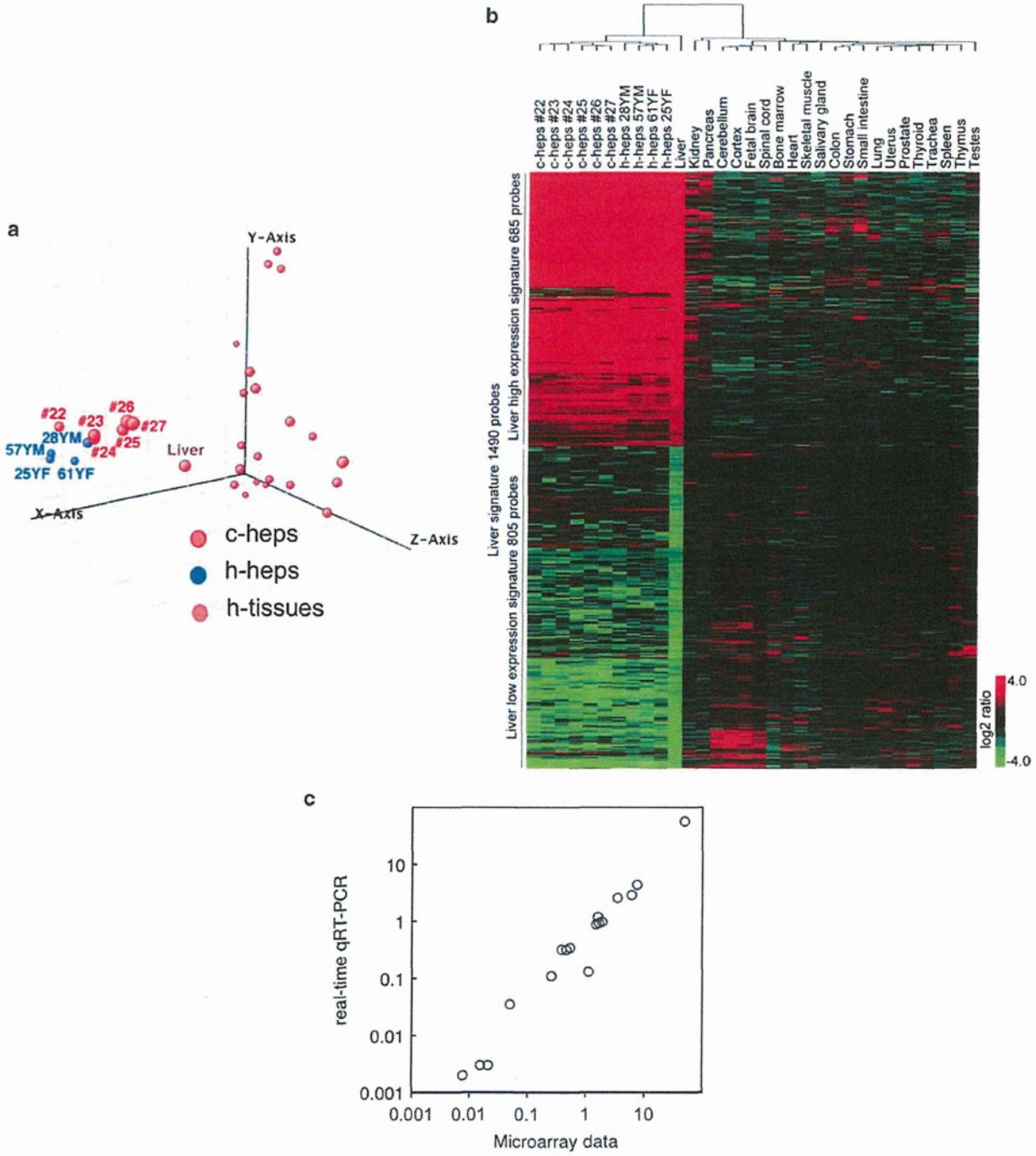

Figure 8 Similarity of gene expression between c-heps and h-heps. (**a**) PCA of c-heps, h-heps, and 22 h-organs or tissues. (**b**) Cluster analysis using the 685 liver high signature probes and the 805 liver low signature probes for c-heps, h-heps, and 22 h-tissues. (**c**) Comparison of the gene expression profiles of chimeric and human hepatocytes using microarray and real-time qRT-PCR analyses. The ratios of gene expression in c- and h-heps, as obtained from the microarray analysis and real-time qRT-PCR, were compared for 17 genes. These data were well correlated.

and liver are highly similar, particularly in the liver high signature probes, but the differences in the expression levels of the liver low signature probes resulted in the clear distinction of the c-hep samples and h-hep samples with the 'normal' liver.

Microarray analysis showed that 191 (170 genes) and 436 (320 genes) probes were significantly (>2 times) higher and lower, respectively, in c-heps than in h-heps. These genes may be up- and down-regulated in the chimeric mouse livers, probably by mismatched receptor–ligand combinations

Table 3 Blood chemistry of chimeric, uPA/SCID, and uPA (wt/wt)/SCID mice

Sex		Chimeric		uPA/SCID	SCID	Human (reference value,
		Male	Female	Male	Male	Male and female)
Age (w)		13.4 ± 0.9	12.0 ± 1.9	12.0 ± 0.0	11.0 ± 0.0	—
Body weight		17.3 ± 2.3	17.6 ± 1.7	17.4 ± 0.3	27.3 ± 0.9	—
n		*5*	*5*	*5*	*3*	—
GOT	U/l	214.6 ± 75.1**[a]	126.8 ± 72.5	367.6 ± 107.7**[b]	44.0 ± 23.3	20–48[c]
GPT	U/l	98.6 ± 16.8*[a]	58.6 ± 18.0	176.4 ± 28.9**[b]	44.3 ± 37.7	10–40[c]
GGT	U/l	23.0 ± 4.6**[a]	15.0 ± 3.9	1.2 ± 0.4	3.7 ± 4.6	0–30[c]
CHE	U/l	396.8 ± 80.2**[a]	282.2 ± 34.1	42.6 ± 8.0**[b]	18.0 ± 5.2	660–1620[d]
BUN	mg/dl	27.3 ± 4.0	23.2 ± 4.6	24.6 ± 9.1	25.3 ± 3.9	8–23[c]
TCHO	mg/dl	88.0 ± 25.8	69.6 ± 18.7	56.8 ± 6.8**[b]	83.3 ± 2.5	<200[c]
HDL-c	mg/dl	20.2 ± 3.4**[a]	18.8 ± 3.7	52.4 ± 7.0**[b]	72.7 ± 6.8	35–80[c]
TG	mg/dl	129.2 ± 24.6	133.2 ± 13.8	82.2 ± 11.0	99.3 ± 10.2	10–190[c]
TBIL	mg/dl	0.4 ± 0.1	0.4 ± 0.0	0.5 ± 0.2	0.6 ± 0.5	0.3–1.2[c]
GLU	mg/dl	154.6 ± 21.6	148.8 ± 31.9	116.4 ± 30.5	154.7 ± 14.2	70–110[c]
ALB	g/dl	3.0 ± 0.4*[a]	2.4 ± 0.1	1.7 ± 0.3	2.2 ± 0.3	3.5–5.0[c]
TP	g/dl	5.0 ± 0.7	4.2 ± 0.3	3.5 ± 0.7*[c]	5.3 ± 0.6	6.0–8.0[c]

[a]Chimeric mouse (male) *vs* SCID mouse (male).
[b]uPA/SCID mouse (male) *vs* SCID mouse (male).
[c]Reference number.[21]
[d]Reference number.[22]
*$P<0.05$, **$P<0.01$.

because of species differences. For example, h-heps were considered to be deficient in growth hormone (GH) because the hGH receptor (hGHR) was unresponsive to mouse GH.[26] Human insulin-like growth factor 1 (IGF-1) was undetectable in chimeric mouse sera.[17,27] We recently identified 4 downregulated and 14 upregulated genes in the chimeric mouse livers when they were treated with hGH.[17] In this microarray analysis, the expression level of fatty acid desaturase 1 (FADS1, c-heps/h-heps ratio: 20.225) was significantly higher in c-hep than in h-heps (Supplementary Table 3). Meanwhile, the expression levels of IGF-1 (c-heps/h-heps ratio: 0.002), suppressors of cytokine signaling 2 (SOCS2; 0.012 and 0.030), nicotinamide *N*-methyltransferase (NNMT; 0.025 and 0.019) chromosome 5 open reading frame 13 (C5orF13; 0.345), solute carrier family 16, member 1(SLC16A1; 0.485 and 0.432), steroid-5-α-reductase, and α-polypeptide 1 (SRD5A1; 0.486 and 0.461) were significantly lower in c-heps (Supplementary Table 3). Consequently, 1 of 170 genes and 6 of 320 genes were up- and down-regulated in c-heps, respectively, because of the lack of hGH in the sera.

Biochemical testing of the chimeric mouse sera revealed high GOT and GPT levels in chimeric and uPA/SCID mice, probably because of m-hep damage caused by uPA expression.[2,28] CHE was higher in chimeric mice than in uPA/SCID and SCID mice, which may be a result of the influence of typically higher h-hep CHE levels. Serum HDL-c levels are higher in mice than in humans, because mice lack cholesterol ester transport proteins that convert HDL-c to LDL-c.[29] HDL-c was lower in the chimeric mice than in the uPA/SCID mice, SCID mice, and humans. At present, the reason for the low HDL-c levels in the chimeric mice is not clear. Further investigations are needed to resolve this question.

We conclude that the chimeric mouse livers showed nearly normal morphology and expressed most genes at similar levels as normal human livers.

Supplementary Information accompanies the paper on the Laboratory Investigation website (http://www.laboratoryinvestigation.org)

ACKNOWLEDGEMENTS

A part of this research was supported by the Yoshizato Project of the Cooperative Link of Unique Science and Technology for Economic Revitalization (CLUSTER), Japan. We thank Y Yoshizane and R Inoue from PhoenixBio, and H Kohno, Y Matsumoto, and S Nagai from CLUSTER for their technical assistance. We also thank H Duimel, University Maastricht, for preparation of the SEM specimen.

DISCLOSURE/CONFLICT OF INTEREST

The authors declare no conflict of interest.

1. Dalvie D, Obach RS, Kang P, *et al.* Assessment of three human in vitro systems in the generation of major human excretory and circulating metabolites. Chem Res Toxicol 2009;22:357–368.